Highlights of Vehicles

ISSN 2696-8347, A Peer-Reviewed Open Access Journal by Highlights of Science
https://www.hos.pub/ho/vehicles

Dynamic Parameter Identification of a Bicycle Using Sliding Mode Observer and Particle Swarm Optimization

by Hocine Imine, Tarek Madani and Murad Shoman

Cite this Article

Imine, H., Madani, T., & Shoman, M. (2025). Dynamic Parameter Identification of a Bicycle Using Sliding Mode Observer and Particle Swarm Optimization. *Highlights of Vehicles*, *3*(2), 15–29. https://doi.org/10.54175/hveh3020002

Highlights of Science

Publisher of Peer-Reviewed Open Access Journals
https://www.hos.pub
Barcelona, Spain

Article

Dynamic Parameter Identification of a Bicycle Using Sliding Mode Observer and Particle Swarm Optimization

Hocine Imine [1,*], **Tarek Madani** [2], **Murad Shoman** [1]

[1] Laboratoire Perceptions, Interactions, Comportements Simulations des usagers de la route et de la rue (PICS-L), Components and Systems Department (COSYS), Gustave Eiffel University, Champs sur Marne 77420, France
[2] Laboratoire Images, Signaux et Systèmes Intelligents, Université Paris-Est Créteil, France
* For correspondence: hocine.imine@univ-eiffel.fr

Abstract The aim of the present work is to identify the unknown dynamic parameters of a bicycle using a sliding mode observer and Particle Swarm Optimization (PSO) approaches. The estimation of bicycle dynamics requires a good knowledge of dynamic parameters such as damping coefficient, spring stiffness, and unsprung masses, among others. In this paper, suspension stiffness and damping coefficient have been identified using the Least Squares Method and compared with those obtained using the PSO technique. Real-time tests have been carried out on an instrumented bicycle equipped with various sensors to measure its dynamics. The measures coming from these sensors have been considered to validate the estimation tools. However, only the vertical wheel displacement measurements have been used to perform the observer. Experimental results are presented and discussed to demonstrate the quality of the proposed approach.

Keywords bicycle modeling; sliding mode observer; particle swarm optimization; identification

1. Introduction

In order to improve cycling safety and foster the peaceful coexistence of cyclists and other road users in urban spaces, it is crucial to consider behavioral aspects in terms of bicycle control and the similarity of behavior exhibited in real situations [1,2]. Knowledge of the physical parameters of a bicycle is essential for finer and more accurate modeling of the bicycle. This helps study the interaction between bicycles and road surface characteristics and geometries, and their effect on cyclist behavior. However, these parameters are generally not well known due to a lack of information from manufacturers or the difficulty in measuring some of them. Researchers working in this field use several techniques to address this problem: simulating the model by neglecting a certain number of parameters, using parameters found in the literature without knowing the conditions under which these parameters were determined, or using parametric identification methods from the field of automatic control. We used the last approach in this work. Indeed, the modeling of a bicycle that we carried out in our previous work on modeling and simulation of bicycle dynamics published in [3] and on subjective validity of bicycle simulators published in [4,5], was based on physical parameters found in the literature. Besides, few works have been published on bicycle modeling with precise values of mechanical parameters [6–8]. Therefore, in this paper, we develop an original method to identify parameters such as the damping coefficient and stiffness using Particle Swarm Optimization (PSO) combined with the High Order Sliding Mode observer (HOSM). We show that HOSM is necessary to estimate in finite time the positions, speeds, and accelerations of the bicycle [9,10]. In the absence of external disturbances, existing tools and methods, such as Kalman filters or Luenberger observers, can be directly applied for asymptotic reconstruction of the system states. However, in the presence of disturbances, standard techniques are not accurate; the Luenberger observer can only ensure convergence to a bounded region near the real value of the state. Sliding mode-based observers are presented as an alternative for the observation of perturbed systems. In particular, HOSM-based observers are successful for state observation of perturbed systems due to their high precision and robust behavior with respect to parametric uncertainties. Moreover, partial or complete knowledge of the system model allows for the application of techniques for parametric or disturbance reconstruction.

Some previous work had already combined both techniques, HOSM and PSO in different manners. For example, in [11], the authors used a sliding mode controller (SMC) in order to

Received: 7 October 2024
Accepted: 11 July 2025
Published: 12 September 2025

Academic Editor
Nicola Bosso, Politecnico di Torino, Italy

control the dynamics of the Quadrator vehicle. PSO is developed here to solve the tuning problem of SMC. The authors in [12] have applied the same methodology in order to optimize SMC parameters by using PSO for an autonomous vehicle.

A new approach and application are highlighted in this paper. Actually, the concept of HOSM is applied in order to state observation of a bicycle, thereby enhancing the precision and robustness of dynamic variables estimation. Indeed, HOSM control excels in managing systems with significant uncertainties and disturbances by using higher-order derivatives to maintain robustness. This technique presents many advantages, especially for modeling the complex dynamics of bicycles. By enabling finite-time estimation of dynamic variables, we propose to use the PSO algorithm to identify unknown parameters. This technique, inspired by the social behaviors of birds and fish, is effective in exploring large search spaces and converging to optimal solutions, making it well-suited for parameter identification in complex systems. Previous studies have demonstrated the effectiveness of PSO in various applications [13–17], and this work builds on those findings by integrating PSO into parameter estimation for bicycle models.

The paper is structured as follows: the first section provides a brief overview of different bicycle models; the second part is devoted to bicycle modeling; in the third part, a third-order observer is developed to estimate dynamic variables; the fourth part focuses on parameter identification using the PSO method; the fifth part describes the experimentation and discusses the validation results; and in the last part, the conclusion and some perspectives are given.

2. Bicycle Modeling

In order to modelize a bicycle, researchers deployed the theoretical physical approach, such as Lagrangian, Euler equations, or the detailed nonlinear Whipple scientific description [6,7]; for example, Whipple [8] used the Linear Quadratic Regulator (LQR) algorithm to analyze the bicycle mathematical model. This method is considered accurate, but time-consuming at the same time. For a straightforward and time-efficient modeling, the classical single-track model could be an alternative [18]. The bicycle mathematical model aims to reproduce the dynamics of a bicycle, in simulation or in a real environment. The geometrical and physical parts of the bicycle are divided as follows: the front part includes the steering axis, the front fork, the front wheel, and a fraction of the cyclist's mass; and the rear part includes the frame, the rear wheel, and the other fraction of the cyclist's body mass. The reactions of total mass are modeled by springs representing the tire's stiffness (k_F and k_R) and damping coefficients (B_F and B_R). The fractions of the bicycle-rider-system mass are m_F and m_R. Distances from the center of gravity to the center of the front wheel and rear wheel are represented by l_F and l_R, respectively. The bicycle has no suspension system, and the pitch angle effect is neglected. The road profile is represented by the variables u_F and u_R. The developed model for this work is shown in Figure 1.

The vertical acceleration values, $\ddot{z}_F$ and $\ddot{z}_R$, of the front and rear wheel respectively, are obtained as follows:

$$\begin{cases} \ddot{z}_F = \dfrac{k_F(u_F - z_F) + B_F(\dot{u}_F - \dot{z}_F)}{m_F} \\ \ddot{z}_R = \dfrac{k_R(u_R - z_R) + B_R(\dot{u}_R - \dot{z}_R)}{m_R} \end{cases}, \tag{1}$$

where z_F and z_R are the vertical displacements of the Center of Gravity (COG) of the front and rear parts respectively, and u_F and u_R are the front and rear values of the road profile.

The normal forces F_{nF} and F_{nR} acting on the wheels are calculated as follows:

$$\begin{cases} F_{nF} = F_{cF} + k_F(u_F - z_F) + B_F(\dot{u}_F - \dot{z}_F) \\ F_{nR} = F_{cR} + k_R(u_R - z_R) + B_R(\dot{u}_R - \dot{z}_R) \end{cases}, \tag{2}$$

where F_{cF} and F_{cR} are the static forces due to the weights of the wheels of the bicycle-rider system applied to the front and rear wheel. They were calculated by applying the equilibrium equation, assuming the bicycle-rider mass m is equal to 85 kg, F_{cF} and F_{cR} are 230 N and 630 N, respectively.

We assume that the front and rear tire vertical stiffness are equal ($k_F = k_R = k$) and the damping coefficients of the front and rear wheel, $B_F = B_R = B$. Tyre width is neglected.

The roll angle (ϕ) of the bicycle among the *x*-axis can be calculated using the speed v_x and radius of curvature R_c [19], as follows:

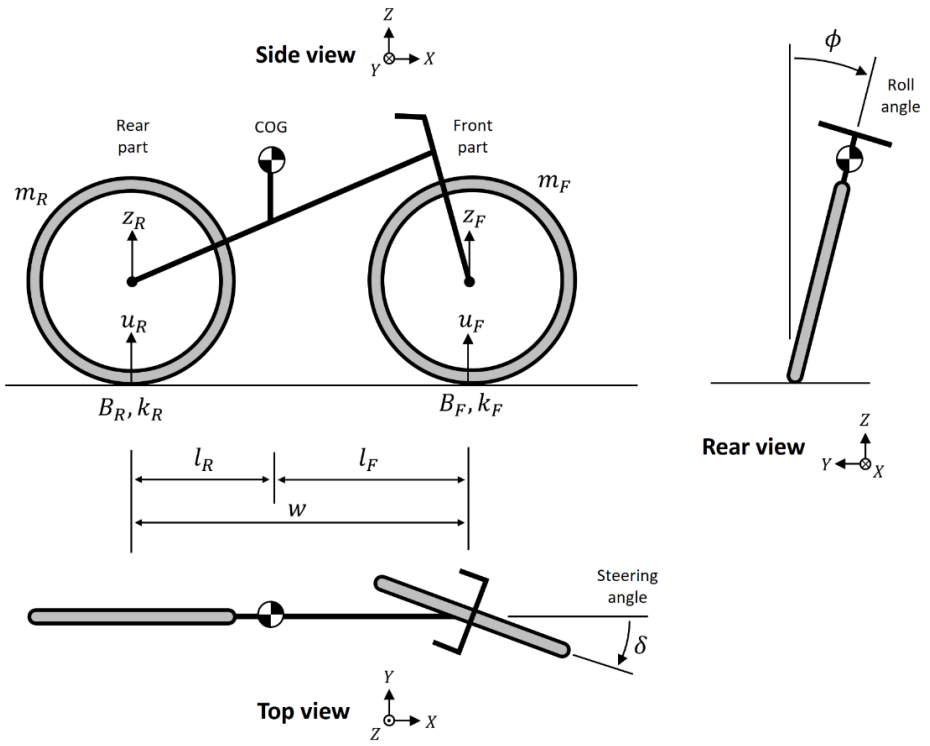

Figure 1. Side view of the bicycle model, divided into two parts: the front and the rear.

$$\phi = \arctan\left(\frac{{v_x}^2}{gR_c}\right). \tag{3}$$

The roll acceleration ($\ddot{\phi}$) is calculated using the mass and rotation matrices as in Equation (4):

$$\ddot{\phi} = r_{31}\phi + r_{32}\delta + r_{34}v_x\dot{\psi} + r_{36}v_x\dot{\delta} - \frac{m_{13}v_y + m_{23}\ddot{\psi} + m_{34}\ddot{\delta}}{m_{33}}, \tag{4}$$

with v_x and v_y are respectively the longitudinal and lateral speed of the bicycle, and

$$r_{31} = (m_F j + m_R h)g, \tag{5}$$

where $\dot{\psi}$ is yaw rate, $\dot{\delta}$ is a derivative of the steering angle, *j* and *h* are the vertical components of the center of gravity for the front and rear part of the bicycle, respectively, and *g* is the gravitational acceleration.

The parameter r_{32} is calculated in Equation (6):

$$r_{32} = m_F eg - \eta F_{nF}, \tag{6}$$

where e is the perpendicular distance between the center of gravity of the front part and the fork and η is the bicycle trail.

$$r_{34} = -m_F j - m_R h - \frac{I_{yR_F}}{R_F} - \frac{I_{yR_R}}{R_R}, \tag{7}$$

where I_{yR_F} and I_{yR_R} are the moments of inertia around the *y*-axis for the front and rear wheel respectively. R_F and R_R are the radii of the front and rear wheels.

$$r_{36} = -\frac{I_{yR_F}}{R_F cos\epsilon}, \tag{8}$$

where ϵ is the bicycle caster angle (i.e., the angular displacement of the steering axis from the vertical axis of a steered wheel).

$$\begin{cases} m_{13} = m_F j + m_R h \\ m_{23} = m_F jk - C_{xzGR} + (I_{zGF} - I_{xGF})\sin\epsilon\cos\epsilon \\ m_{33} = m_F j^2 + m_R h^2 + I_{xGR} + I_{zGF}\sin\epsilon^2 + I_{xGF}\cos\epsilon^2 \\ m_{34} = m_F \epsilon j + I_{zGF}\sin\varepsilon \end{cases}. \tag{9}$$

3. Sliding Mode Observer Design

In order to evaluate the rollover risk, high high-order sliding mode observer is developed to estimate in finite time the state variables and identify unknown parameters [9,10].

To develop HOSM, the system Equation (1) is rewritten as follows:

$$M(q)\ddot{q} + B(q,\dot{q})\dot{q} + K(q) = F_g, \tag{10}$$

where $M \in \Re^{2\times 2}$ is the inertia matrix (mass matrix), $B \in \Re^{2\times 2}$ is the matrix taking into account the damping effects, $K \in \Re^2$ is the spring's stiffness vector and $F_g \in \Re^2$ is the generalized forces composed of the road profile u and its derivative $\dot{u}$. The coordinates variable vector $q \in \Re^2$ is defined by $q = [q_1, q_2]^T$, where $q_1 = z_F$ and $q_1 = z_R$ are respectively the front and rear wheel vertical displacements.

In state space form, the system Equation (10) can be rewritten as:

$$\begin{cases} \dot{x}_{11} = x_{21} \\ \dot{x}_{21} = a_1\varphi(x_{11}, x_{21}) \\ \dot{x}_{12} = x_{22} \\ \dot{x}_{22} = a_2\varphi(x_{12}, x_{22}) \end{cases}, \tag{11}$$

where $x = (x_1, x_2)^T = (q, \dot{q})^T \in \Re^4$ is the state variables vector such that $x_1 = [x_{11}, x_{12}]^T = [z_F, z_R]^T$ and $x_2 = [\dot{x}_{11}, \dot{x}_{12}]^T = [\dot{z}_F, \dot{z}_R]^T$, $y = x_1 = [z_F, z_R]^T$ is the measured outputs vector of the system. The vectors of parameters are represented by $a_1 = [k/m_F \; B/m_F]$ and $a_2 = [k/m_R \; B/m_R]$, and the vectors are

$$\begin{cases} \varphi(x_{11}, x_{21}) = [(u_F - z_F), (\dot{u}_F - \dot{z}_F)]^T \\ \varphi(x_{12}, x_{22}) = [(u_R - z_R), (\dot{u}_R - \dot{z}_R)]^T \end{cases}.$$

To simplify the system, the vector of unknown parameters a is introduced:

$$a = \begin{cases} [a_{11}, a_{21}] = \left[\dfrac{k}{m_F} \dfrac{B}{m_F}\right] \\ [a_{12}, a_{22}] = \left[\dfrac{k}{m_R} \dfrac{B}{m_R}\right] \end{cases}.$$

To be able to estimate the state variables, the following observer is developed, and the convergence is proved [9,10]:

$$\begin{cases} \dot{\hat{x}}_1 = \hat{x}_2 - \lambda_0 \nabla(v_1) Sign(v_1) \\ \dot{\hat{x}}_2 = \hat{x}_3 - \lambda_1 \nabla(v_2) Sign(v_2), \\ \dot{\hat{x}}_3 = -\lambda_2 Sign(v_3) \end{cases} \tag{12}$$

where $\hat{x}_1$, $\hat{x}_2$ and $\hat{x}_3$ are respectively the estimates of x_1, x_2 and $\dot{x}_2$; where $(x_1, x_2) = (x_{11}, x_{21})$ or $(x_1, x_2) = (x_{12}, x_{22})$, $\tilde{x}_i = \hat{x}_i - x_i$ $(i = 1, \ldots, 3)$ is the estimation error of the variable x_i, λ_0, λ_1, and λ_2 are the observer gains, $v_1 = \tilde{x}_1 = \hat{x}_1 - x_1$, $v_2 = \hat{x}_2 - \dot{\hat{x}}_1$ and $v_3 = \hat{x}_3 - \dot{\hat{x}}_2$.

We set

$$\dot{\hat{x}}_3 = \bar{a}\varphi(\hat{x}_1, \hat{x}_2), \tag{13}$$

where $\bar{a}$ represents the vector of nominal values of the vector parameters a_1 or a_2. $\tilde{a} = a - \bar{a}$ is the estimation error of the vector parameters a.

By setting $\nabla(v_1) = |v_1|^{2/3}$ and $\nabla(v_2) = |v_2|^{1/2}$, we define the functions $Sign$ and $\nabla(\;)$ as follows:

$$\begin{cases} \nabla(v_1) = diag\{|v_{1_1}|^{2/3}, |v_{1_2}|^{2/3}\} \\ \nabla(v_2) = diag\{|v_{2_1}|^{1/2}, |v_{2_2}|^{1/2}\} \\ Sign(v_1) = [Sign(v_{i1}), Sign(v_{i2})]^T, i = 1,2,3 \end{cases}. \tag{14}$$

The observer defined in the system Equation (12) permits to estimate in real time positions, velocities, and accelerations of the system. The jerk of the system is bounded, and it satisfies the inequality:

$$f^+ \geq 2|\ddot{x}_{1i}|, i = 1,2,3, \tag{15}$$

where f^+ is some known positive scalar.

Remark 1. *When the accelerations in the mechanical system are bounded, the constant f^+ can be found as the double maximal possible jerk of the system. Moreover, the estimation constant f^+ does not depend on the nominal elasticity or control terms. Such assumption of the state boundedness is true as well, if, for example, system (11) is BIBS (Bounded Input, Bounded State) stable, and the control input $u = U(t, x_1, x_2)$ is bounded.*

The bicycle is a dynamic system with a bounded jerk. The derivative of the measured accelerations, namely, the jerk coming from the third derivative of vertical displacement, are performed in order to prove the condition in Equation (15).

The estimation errors are obtained using Equations (11) and (12) as follows:

$$\begin{cases} \dot{\tilde{x}}_1 = x_2 - \hat{x}_2 + \lambda_0 \nabla(v_1) Sign(v_1) \\ \dot{\tilde{x}}_2 = \dot{x}_2 - \hat{x}_3 + \lambda_1 \nabla(v_2) Sign(v_2), \\ \dot{\tilde{x}}_3 = \ddot{x}_2 + \lambda_2 Sign(v_3) \end{cases} \tag{16}$$

where $\dot{x}_2 = M^{-1}\left(F_g - B(x_1, x_2)x_2 - K(x_1)\right)$.

Chosen the i^{th} components of $\lambda^i{}_0$, $\lambda^i{}_1$ and $\lambda^i{}_2$ as: $\lambda^i{}_0 = 3\sqrt[3]{f^+}$, $\lambda^i{}_1 = 1.2\sqrt[2]{f^+}$, $\lambda^i{}_2 = 1.1 f^+$, the estimation errors $\tilde{x}_1, \tilde{x}_2, \tilde{x}_3$ converge in finite time t_0 toward 0.

Then, after the convergence of the differentiator, the equality $\dot{\tilde{x}}_2 = \dot{x}_2 = M^{-1}(F_g - B(x_1, x_2)x_2 - K(x_1))$ holds, and given the equivalence between Equations (11) and (12), the following equality is satisfied:

$$M^{-1}\left(F_g - B(x_1, x_2)x_2 - K(x_1)\right) - \hat{x}_3 + \lambda_1 \nabla(v_2) Sign(v_2) = 0. \tag{17}$$

The third term of the above-mentioned equality is equal to zero as a result of the differentiator convergence, so it is possible to obtain the equivalent output injection as:

$$z_{eq} = \hat{x}_3 = M^{-1}\left(F_g - B(x_1, x_2)x_2 - K(x_1)\right). \tag{18}$$

In this case, $\hat{x}_3$ is a continuous term, and no filtration is required to obtain the equivalent output injection. This is an important fact, because given the finite time convergence of the differentiator, it's possible now to reconstruct in finite time the equivalent output injection. Moreover, the variable $\hat{x}_3$ is not affected by any filtration process, hence $\hat{x}_3$ is an exact estimation of $M^{-1}(F_g - B(x_1, x_2)x_2 - K(x_1))$.

More details about the convergence study of this observer can be found in [20].

4. Parameters Identification Using the Least Squares Method

In order to identify the parameters, Least Squares Method (LS) is applied using Equation (19):

$$z_2 = \hat{x}_3 = \tilde{a}\varphi(x_1, x_2) = M^{-1}\left(F_g - B(x_1, x_2)x_2 - K(x_1)\right). \tag{19}$$

Considering the unknown parameters vector $\tilde{a} = a - \bar{a}$ as a constant vector and in order to identify it, a linear regression algorithm, namely, the least squares method, is applied [21–23].

The time integration is given by:

$$\frac{1}{t}\int_0^t z_2(\sigma)\,\varphi(\sigma)^T d\sigma = \tilde{a}\frac{1}{t}\int_0^t \varphi(\sigma)\varphi(\sigma)^T d\sigma. \tag{20}$$

The vector $\tilde{a}$ is then estimated by:

$$\hat{\tilde{a}} = \left[\int_0^t z_2(\sigma)\,\varphi(\sigma)^T d\sigma\right]\left[\int_0^t \varphi(\sigma)\varphi(\sigma)^T d\sigma\right]^{-1}, \tag{21}$$

where $\hat{\tilde{a}}$ is the estimation of $\tilde{a}$.

Let us define $\Gamma = \left[\int_0^t \varphi(\sigma)\varphi(\sigma)^T d\sigma\right]^{-1}$, and its derivative gives $\dot{\Gamma} = -\Gamma\varphi(\sigma)\varphi(\sigma)^T\Gamma$. The derivative of the vector $\hat{\tilde{a}}$ using Equation (21) provides:

$$\dot{\hat{\tilde{a}}} = \left[\int_0^t z_2(\sigma)\,\varphi(\sigma)^T d\sigma\right]\dot{\Gamma} + z_2\varphi^T\Gamma. \tag{22}$$

Replacing by its value given before and using Equation (21), it follows:

$$\dot{\hat{\tilde{a}}} = -\hat{\tilde{a}}\varphi\varphi^T\Gamma + z_2\varphi^T\Gamma = \left(-\hat{\tilde{a}}\varphi + z_2\right)\varphi^T\Gamma. \tag{23}$$

This ensures the asymptotic convergence of $\hat{\tilde{a}}$ toward $\tilde{a}$ and, therefore, this allows the identification of the real value of the vector.

5. Parameters Identification Using the PSO Method

The PSO technique is inspired by the flight movement of birds [13,14]. Its iterative algorithm is based on a random initialization of a flock of birds, called particles, in the searching space. The velocity of each particle is updated at each iteration by considering its inertia and the influence of its best position, as well as the best position of the best individual. Naturally, the particle flies to the optimal position by following an atypical way. Let $\theta \in \Re^4$ be the vector of unknown parameters to be identified, such as:

$$x_{m3} = \Psi(x_{m1}, x_{m2}, u, \dot{u})\theta, \tag{24}$$

where $x_{m1} \in \Re^2$, $x_{m2} \in \Re^2$, and $x_{m3} \in \Re^2$ represent the position, velocity, and acceleration of the model, respectively, approximating the real position $x_1 = [z_F, z_R]^T$, the real velocity $x_2 = [\dot{z}_F, \dot{z}_R]^T$, and the real acceleration $x_3 = [\ddot{z}_F, \ddot{z}_R]^T$, respectively; $u = [u_F, u_R]^T$ is the input road profile, $\dot{u} = [\dot{u}_F, \dot{u}_R]^T$ is the derivative of the road profile, $\theta = \left[\frac{k_F}{m_F}, \frac{B_F}{m_F}, \frac{k_R}{m_R}, \frac{B_R}{m_R}\right]^T$ is the parameter vector, and $\Psi(x_{m1}, x_{m2}, u, \dot{u}) \in \Re^{2\times 4}$ is a regression function based on Equation (1).

In this section, the PSO is employed to estimate the vector θ. To carry out this estimation, a dataset is required, which is constructed from the variables x_1, x_2, x_3, u, and $\dot{u}$. These variables are assumed to be known a priori, meaning their values are available beforehand, typically obtained through measurements, simulations, or prior knowledge. The availability of accurate and representative data is crucial for ensuring the reliability and convergence of the estimation process.

The main objective is to estimate iteratively the vector θ by using the PSO method. Suppose that the position and the velocity of the *i*-th PSO particle are represented by $X_i \in \Re^4$ and $V_i \in \Re^4$, respectively. The purpose of the identification is to calculate the optimal parameters to ensure a better fit of the model. This means that the calculated system output approximates the actual system output as closely as possible. The closer these two values are, the better the effect of the parameter adjustment. In order to ensure this, the fitness of the *i*-th particle is evaluated according to the following quadratic objective function:

$$J_i = \int_{t_1}^{t_2} e_i^T W e_i \, dt, \tag{25}$$

where the elapsed time t_1 to t_2 represents the search horizon ($t_2 > t_1 > 0$), $W \in \Re^{6\times 6}$ is a diagonal positive weighting matrix, and the vector $e_i \in \Re^6$ is given by Equation (26):

$$e_i = \begin{bmatrix} x_1 - x_{m1} \\ x_2 - x_{m2} \\ x_3 - \Psi(x_{m1}, x_{m2}, u, \dot{u})X_i \end{bmatrix}. \tag{26}$$

The objective function J_i is minimum when X_i gets as close as possible to θ. So, the system identification is cast into an optimization problem. The minimization procedure is performed via a PSO as shown below.

At the initial iteration $k = 0$, the particles are initialized with random positions $\{X_{1_0}, \ldots, X_{n_0}\}$ and velocities $\{V_{1_0}, \ldots, V_{n_0}\}$ in a bounded search space. For each step k, the best previously visited position (from iteration 0 to k) of the *i*-th particle is noted as its personal best position, denoted by $P_i \in \Re^4$ and the position of the optimum individual of the swarm is noted as the global best position $G \in \Re^4$. The *i*-th particle modifies its movement in the search space by using the following formulas:

$$X_{i_{k+1}} = X_{i_k} + V_{i_k}, \tag{27}$$

and

$$V_{i_{k+1}} = \omega_k V_{i_k} + c_1 \, r_1 \, (P_i - X_{i_k}) + c_2 \, r_2 \, (G - X_{i_k}), \tag{28}$$

where ω_k represents the inertia weight, $r_1, r_2 \in [0,1]$ are uniformly distributed random variables and $c_1, c_2 \in \Re^+$ are weighting constant factors.

Figure 2 illustrates a schematic of the identification technique using the PSO method. The "Model" block simulates the dynamics of the bicycle for each individual in the PSO population, which represents the parameter vector. The discrepancy between the variable x_3 and its model estimate is used to calculate the optimization error. This error is fed back into the algorithm to compute the objective function value. To elaborate further, the PSO method is an evolutionary computation technique inspired by the social behavior of birds flocking or fish schooling. It optimizes a problem by iteratively improving candidate solutions with regard to a given measure of quality or fitness. In this context, the "Model" block's role is crucial as it performs simulations based on the dynamics of the bicycle for each particle (individual) in the swarm. Each particle represents a potential solution characterized by a vector of parameters that define the model's behavior.

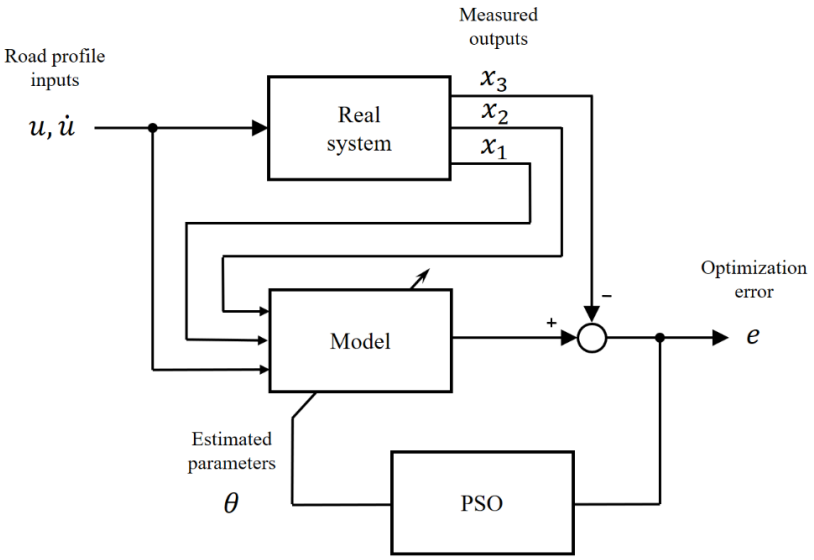

Figure 2. Schematic block diagram of parameter identification using the PSO method.

In the original PSO algorithm [14], the inertial weight ω_k does not change and remains equal to 1 for $\forall k$. In practical applications, the PSO algorithm may pose some problems, such as premature convergence and the balancing around the optimal solution. In order to overcome those problems, various strategies are given in the literature [15,16,24,25] to improve the choice of the inertial weight. In a general manner, the inertial weight should be reduced quickly at the beginning of the process and should be slowly reduced around the optimum. In this paper, a modified PSO method is proposed by introducing the following strategy of the inertial weight:

$$\omega_k = \omega_{\min} + \delta_k \, (\omega_{\max} - \omega_{\min}), \tag{29}$$

where $\omega_{\min} \in \Re^+$ and $\omega_{\max} \in \Re^+$ are the lower and the upper bounds of the inertial weight, respectively, and $\delta_k \in [0,1]$ is a damping factor computed by the following geometric sequence:

$$\delta_{k+1} = \rho \, \delta_k, \tag{30}$$

with $\delta_0 = 1$ and $\rho \in [\rho_{\min}, \rho_{\max}]$ is a uniformly distributed random common ratio such as $0 < \rho_{\min} \leq \rho \leq \rho_{\max} < 1$.

6. Experimentation

6.1. Description of the Test Bench

Experimentation in a real environment is not always the appropriate means, due to its costs, bias related to uncontrolled variables, and risks facing cyclists [26,27]. However, in order to validate the theoretical study and the simulation results, an instrumented bicycle is used, as shown in Figure 3. The bicycle is equipped with several sensors to measure its dynamics, such as the angular speeds, accelerations, and displacements. In addition, as shown in Figure 3, a battery is installed in order to supply power to some sensors, and a USB WSDA 200 key is used in order to communicate with the other sensors to log data on a PC. Many tests have been conducted with the bicycle driving at various speeds on an open road in Stockholm, Sweden. The data

collection was carried out at a frequency of 100 Hz. This frequency was chosen to ensure sufficient temporal resolution for capturing the dynamic behavior of the bicycle model. Some results on the state estimation and parameter identification using the Least Squares method and PSO technic are presented in this section. The static vertical forces are measured before the tests. The measured static front and rear right vertical forces are respectively 225.63 N and 608.22 N. The dynamic parameters of the bicycle are l_F = 0.808 m, l_R = 0.293 m, m_F = 23 kg, and m_R = 63 kg.

Figure 3. The instrumented bicycle used during the experiment. The numbers represent the different sensors mounted on the bicycle are described as follows. 1. SG-LINK-200-OEM + Hall Effect Sensor from Alliantech was used to count the number of rotations per minute (RPM) for the front wheel in order to calculate its angular velocity. The sampling rate was set to 250 Hz. 2. G-link-200 Triaxial accelerometer from AlianTeck is a wireless 3-axis accelerometer with ±2 to ±40 g measurement range. The sampling rate is up to 4096 Hz. 3. GPS (Global Positioning System): Edge 130 plus from Garmin that includes: GPS, GLONASS, and GALILEO systems to detect position in real time. 4. P25 wire-wound potentiometer from RS Pro, it is connected with specially designed cogs and attached to the handlebar to measure the steering angle. The sampling rate is 100 Hz. 5. Inertial Measurement Unit (IMU) unit+ WLAN "Shell" 4.0 Data Logger: from Avisaro, was used as a data logger with a 6 DOF IMU unit (3 axis acceleration/3 axis gyro). The IMU sampling rate was set to 100 Hz. 6. OY1P303P0189 laser scanner, from Wenglor, was used for the continuous measuring of the distance between the top of the rear seat and the road surface. The sampling rate is 30 Hz. 7. K2 powerbank, from PowerOak, was used as a battery to provide power to the laser scanner and the data logger. 8. Speed sensor 2, from Garmin, is a wireless sensor that gives longitudinal velocity. 9. Vector 3 power meter pedals from Garmin provides dual-sensing on both pedals. 10. Cadence sensor 2 from Garmin, was fastened to the left-side crank arm to measure pedal strokes per minute.

6.2. Experimental Results of the Observation

In order to identify unknown parameters, the dynamic variables of the bicycle need to be estimated in a finite time. In this part, some results on estimation variables done by the sliding mode observer (SMO) are shown.

In Figure 4, estimated and measured vertical displacements are compared. We can then appreciate the quality of the estimation using the SMO technic. In the bottom of Figure 4, the vertical speed is also well estimated compared to the measured one with an error close to zero. We notice that there is no chattering in this case, compared to the results obtained by using a first-order observer. This result is confirmed in Figure 5, where the error is calculated for both variables. Indeed, we notice that the maximum error in the vertical displacement is less than 1 mm. While for the estimation of the vertical speed, the maximum error is less than 0.06 m/s.

These results are then used in the next section in order to identify the parameters using the proposed PSO algorithm and the LS method.

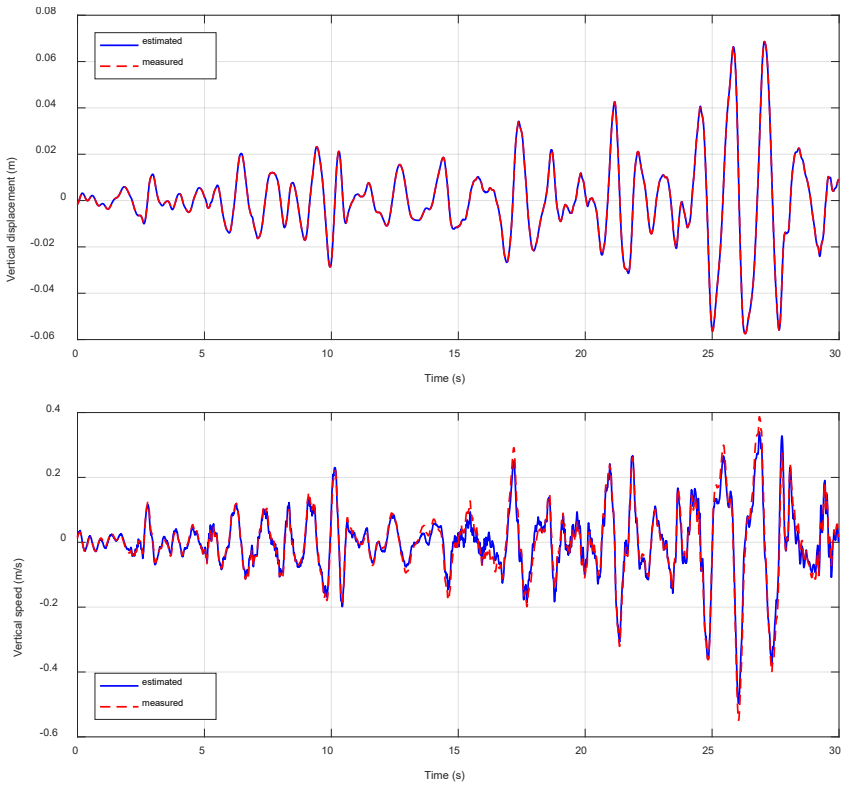

Figure 4. Comparison between estimated variables using SMO and measured ones.

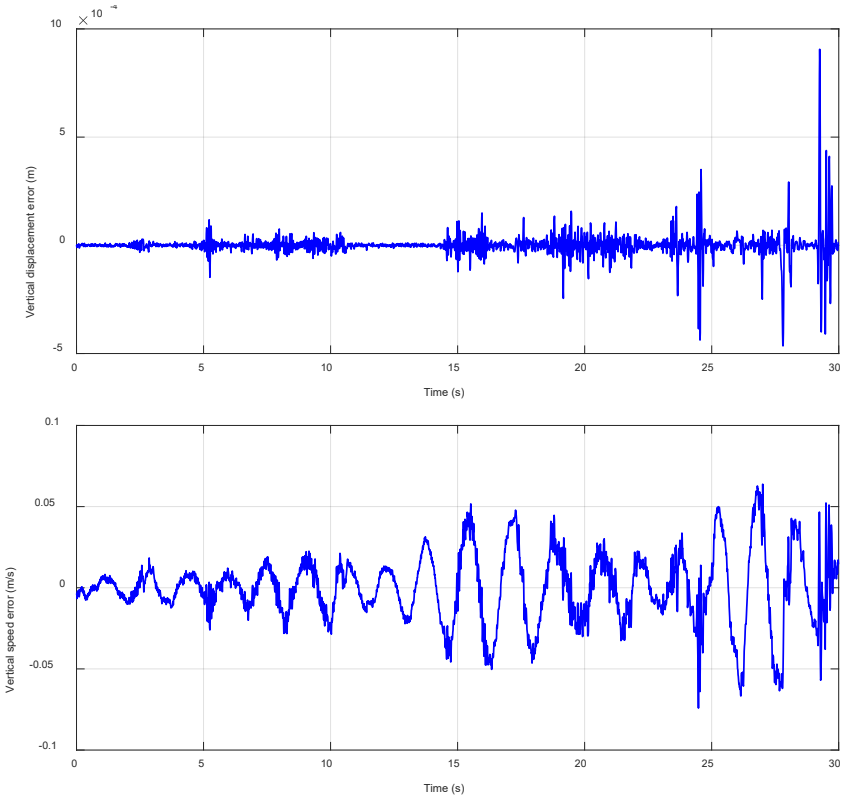

Figure 5. Estimation error of vertical displacement and speed.

6.3. Experimental Results of the Identification

The computational time for the LS method running online is about 1 s. While for PSO method runs offline and according to 20 iterations with 30 individuals, the computational time is about 45 s using Matlab software.

The identified sprung stiffness coefficient and damping using the LS method are equal, respectively, to 110,600 N/m and 1135 N/(m/s). Let us now compare these values to those calculated by the PSO algorithm.

Figure 6 shows the results obtained with a population of 30 particles initialized randomly. The top curve in this figure illustrates the evolution of the best cost optimization criterion. The two lower curves show the evolution of the best positions. It can be seen that the parametric convergence is achieved around the tenth iteration. To ensure robustness, 10 different initial conditions were tested. Based on the cost function curve, the best test corresponds to trial number 7. We notice that the identified stiffness, obtained by the best trial number 7, is about 109,364 Nm, very close to the value identified by the LS method, which is equal to 110,600 Nm. The same remark can be given to the damping coefficient identified by the PSO method, which converges to 1234 N/(m/s), very close to the value identified by LS, namely 1135 N/(m/s).

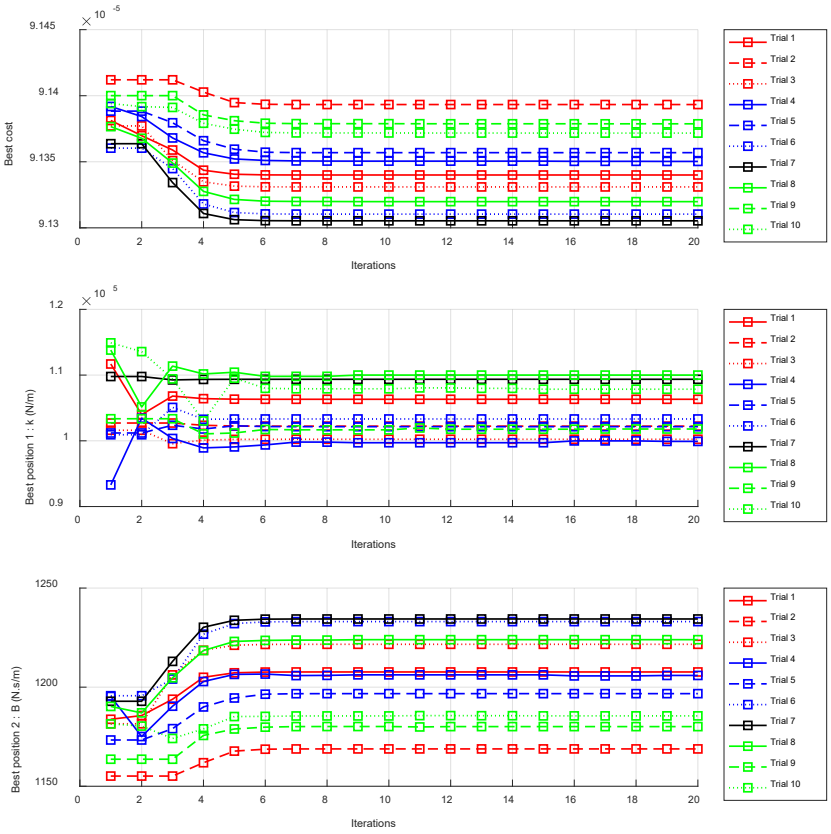

Figure 6. Best cost and best positions 1 and 2.

The parameters identified using the LS method and PSO technique, tested with 10 different initial conditions, are compared in Figure 7. We notice that the identified stiffness is about 106,320 Nm, very close to the value identified by the LS method, which is equal to 110,600 Nm. The same remark can be given to the damping coefficient identified by the PSO method, which converges to 120,767 N/(m/s), very close to the value identified by LS, namely 1135 N/(m/s). The identification results obtained with both techniques are consistent, demonstrating the solidity and reliability of both approaches. Each method, LS and PSO, has its advantages: LS is favored for its simplicity and efficiency in handling linear data, while PSO excels in solving complex and nonlinear problems. Both methods produce aligned results, indicating the robustness of the identification process. The observed variations in values are likely due to variable conditions and parameters in the experiments, influenced by factors such as environmental influences, measurement precision, and specific experimental setup variations. Fluctuations in temperature, electromagnetic interference, or voltage variations can affect measurements. Additionally, the precision of measurement instruments and the positioning of sensors play a crucial role in the accuracy of the results. In summary, although the main results remain reliable and robust, the exact values reflect the nuances of the experimental conditions, highlighting the importance of controlling and documenting these conditions for precise interpretation of the results. This comparative

analysis between LS and PSO highlights the complementarity of the two techniques and their applicability in different experimental contexts, thereby reinforcing confidence in the processes of parameter identification and analysis.

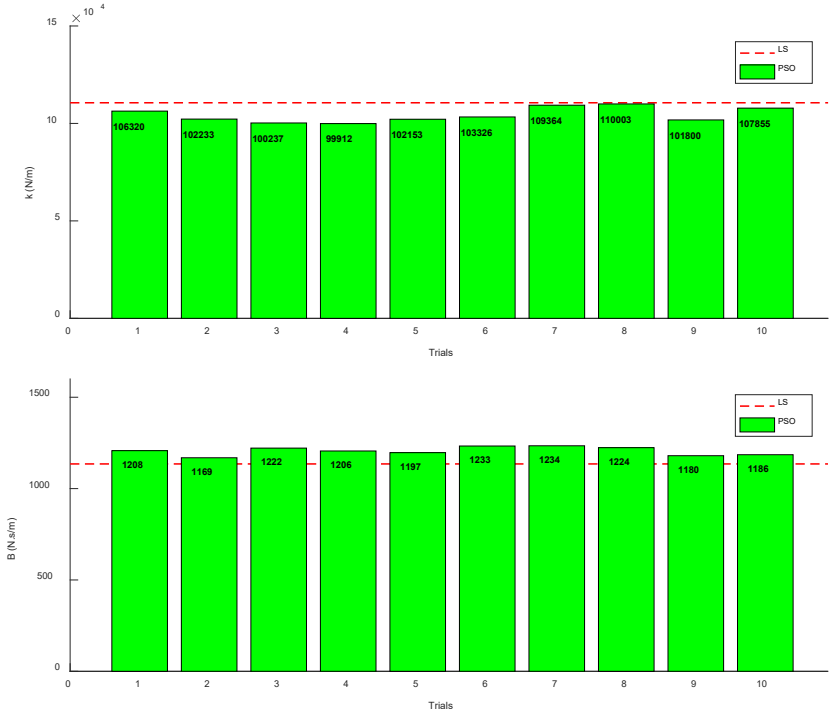

Figure 7. The identified parameters using the LS and PSO methods.

The identified parameters have been used in the model and in the observer defined in Equation (12). The measured vertical displacement is compared to those estimated by the LS and PSO methods by using the respective identified parameters.

The results of Figure 8 show the convergence of the two methods, where the vertical displacement has been estimated with success, with an error close to zero. This important result confirms that the identified parameters obtained by using LS and PSO are reliable. The measured vertical speed is also compared to those estimated by the LS and PSO methods by using the respective identified parameters. The result of this comparison is shown in Figure 9. We remark that by using the parameters identified by both methods, velocity has been well estimated, in finite time and without chattering, compared to the measured one. This is an important and reliable result which proves the accuracy of the identification techniques developed in this paper.

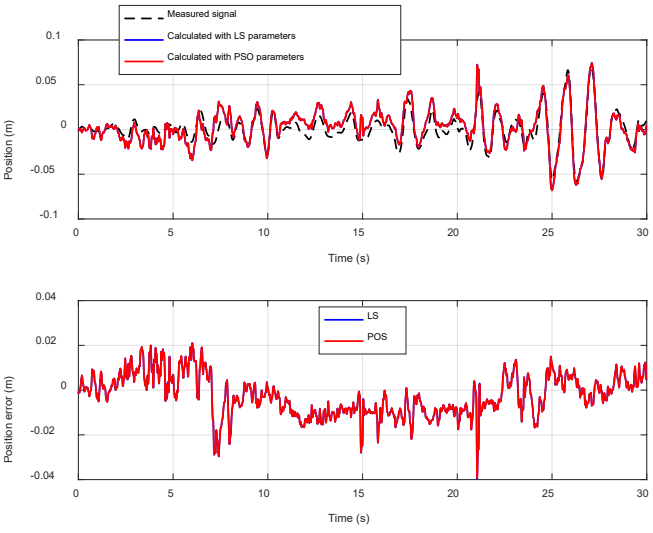

Figure 8. Measured vertical displacement compared to those estimated by the LS and PSO methods.

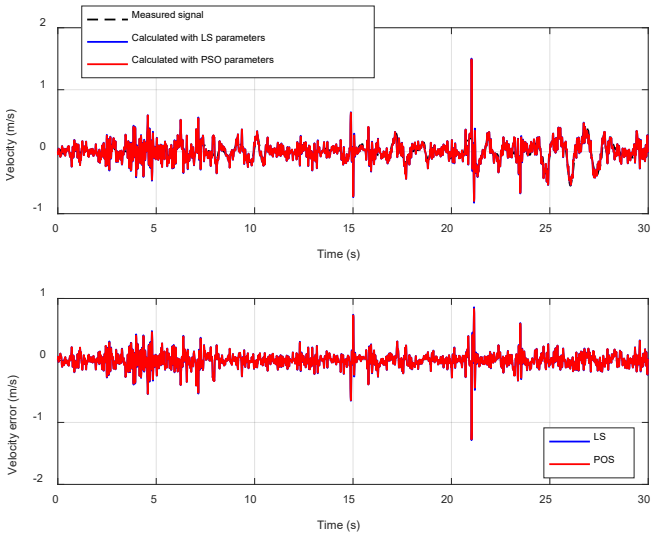

Figure 9. Measured vertical speed compared to those estimated by LS and PSO.

Figure 10 presents the comparison between the measured vertical acceleration and the estimates obtained using the LS and PSO methods, based on their respective identified parameters. Both methods accurately estimate the acceleration. These results validate the effectiveness and precision of the identification techniques proposed in this study.

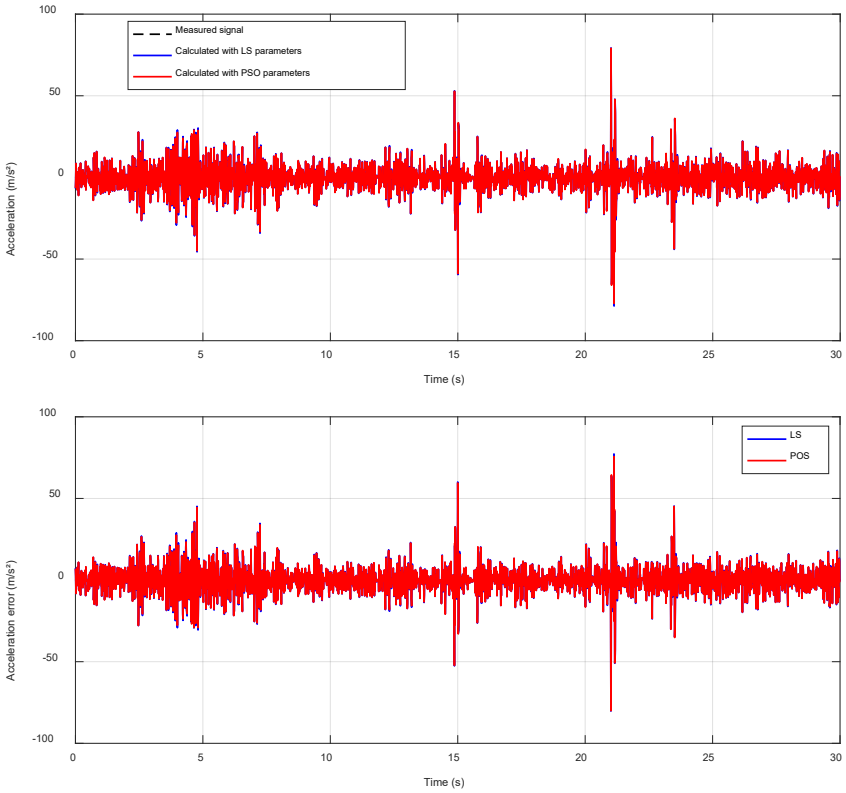

Figure 10. Measured vertical acceleration compared to those estimated by LS and PSO.

Table 1 compares the performance of two estimation methods, LS and PSO, in terms of maximum absolute error and mean square error for position, velocity, and acceleration. A discussion regarding these results is given below:

- For position, both the LS and PSO methods show very similar performance, with maximum absolute errors of approximately 39.53×10^{-3} m for LS and 39.08×10^{-3} m for PSO. The mean square errors are also nearly identical, with LS at 8.949×10^{-5} m/s and

PSO at 8.947×10^{-5} m/s. This indicates that both methods provide very close estimations for the position with minimal discrepancies.

- For velocity, the maximum absolute error is slightly higher for LS (1.286 m/s) compared to PSO (1.273 m/s). The mean square error also shows a similar pattern, with LS having a value of 13.561×10^{-3} m/s² and PSO at 12.895×10^{-3} m/s². While both methods perform well, PSO appears to offer slightly more accurate results in velocity estimation.
- For acceleration, LS shows a higher maximum absolute error (80.242 m/s²) compared to PSO (79.999 m/s²). The mean square errors also reflect this difference, with LS at 70.854 m²/s and PSO at 67.700 m²/s. Again, PSO outperforms LS in terms of accuracy for acceleration estimation, with smaller errors in both the maximum absolute and mean square error.

Overall, the PSO method demonstrates a slightly better performance than the LS method in all three parameters (position, velocity, and acceleration), with smaller errors in both maximum absolute and mean square error. However, the differences are minimal, suggesting that both methods provide reliable and accurate estimations for the system under study.

Table 1. Statistical comparison of the estimation errors.

	Position (m)		**Velocity (m/s)**		**Acceleration (m/s²)**	
Estimation method	Maximum absolute error	Mean square error	Maximum absolute error	Mean square error	Maximum absolute error	Mean square error
LS	39.531×10^{-3}	8.949×10^{-5}	1.286	13.561×10^{-3}	80.242	70.854
PSO	39.084×10^{-3}	8.947×10^{-5}	1.273	12.895×10^{-3}	79.999	67.700

The results show that the PSO algorithm is a powerful technique. It can be used in real situations, even in the presence of noise measurement. The comparison given with the PSO algorithm and the LS method shows the efficiency of the proposed PSO method.

7. Conclusion

In this paper, parameters of a bicycle are identified using a modified PSO method combined with an HOSM observer to estimate in finite time the dynamic variables vector. We have shown in the presented results that after the real-time convergence of the vertical position, velocity, and acceleration of the bicycle using HOSM, the PSO technique was able to identify the stiffness coefficient and damping. Indeed, the comparison between measured variables from sensors and estimated variables demonstrates the robustness of the observer, as well as the effectiveness of the estimation. The quality of identification using the proposed PSO is also evaluated by comparing its results to those obtained from the Least Squares Method. This comparison shows the convergence of these two methods with errors close to zero, as proved in the statistical study. In future work, as mentioned in the introduction and bicycle modelling part, other parameters need to be identified for better convergence of the model. This can be possible by using the two approaches developed in this paper. The goal will also be to increase the robustness of the validation of the entire dynamic model of the bicycle. In this case, the lateral model part will be developed in order to identify cornering stiffness coefficients.

Funding

This work is funded by Marie Skłodowska-Curie actions (H2020 MGA MSCA-ITN) within the SAFERUP project under grant agreement number 765057.

Data Availability

The data used to support the findings of this paper are available from the corresponding author upon request.

Author Contributions

H.I. and M.S. developed the dynamic model of bicycle; M.S. conducted the experimentation and analyzed data; H.I. developed the sliding mode observer and LS Method, analyzed data and supervised the work; T.M. developed the PSO method, analyzed data and supervised the work.

Conflicts of Interest

The authors have no conflict of interest to declare.

References

1. Shoman, M., Simone, A., & Vignali, V. (2018). Looking behavior to vertical road signs on rural roads. *MOJ Civil Engineering*, *4*(2), 75–79.
2. Billot-Grasset, A., Amoros, E., & Hours, M. (2016). How cyclist behavior affects bicycle accident configurations? *Transportation Research Part F: Traffic Psychology and Behaviour*, *41*, 261–276.
3. Shoman, M., & Imine, H. (27–30 April 2020). *Modeling and simulation of bicycle dynamics*. The 8th Transport Research Arena TRA 2020, Helsinki, Finland.
4. Shoman, M., & Imine, H. (18–22 October 2020). *Subjective validity of bicycle simulators*. The Ninth International Conference on Advances in Vehicular Systems, Technologies and Applications, Porto, Portugal.
5. Shoman, M., & Imine, H. (2021). Bicycle Simulator Improvement and Validation. *IEEE Access*, *9*, 55063–55076. https://doi.org/10.1109/ACCESS.2021.3071214
6. Owczarkowski, A., Horla, D., Kozierski, P., & Sadalla, T. (29 August–1 September 2016). *Dynamic modeling and simulation of a bicycle stabilized by LQR control*. The 21st International Conference on Methods and Models in Automation and Robotics (MMAR), Miedzyzdroje, Poland. https://doi.org/10.1109/MMAR.2016.7575258
7. He, Q., Fan, X., & Ma, D. (2005). Full bicycle dynamic model for interactive bicycle simulator. *Journal of Computing and Information Science in Engineering*, *5*(4), 373–380. https://doi.org/10.1115/1.2121749
8. Whipple, F. J. (1899). The stability of the motion of a bicycle. *The Quarterly Journal of Pure and Applied Mathematics*, *30*, 312–321.
9. Fridman, L., Levant, A., & Davila, J. (13–15 December 2006). *High-Order Sliding-Mode Observation and Identification for Linear Systems with Unknown Inputs*. The 45th IEEE Conference on Decision and Control, San Diego, CA, USA. https://doi.org/10.1109/CDC.2006.377385
10. Imine, H., Benallegue, A., Madani, T., & Srairi, S. (2014). Rollover risk prediction of heavy vehicle using high order sliding mode observer. *IEEE Transactions on Vehicular Technology*, *63*(6), 2533–2543. https://doi.org/10.1109/TVT.2013.2292998
11. Baldini, A., Ciabattoni, L., Felicetti, R., Ferracuti, F., Freddi, A., Monteriù, A., et al. (2017). Particle swarm optimization based sliding mode control design: Application to a quadrotor vehicle. In S. Vaidyanathan & C. H. Lien (Eds.), *Applications of Sliding Mode Control in Science and Engineering* (pp. 143–169). Springer, Cham. https://doi.org/10.1007/978-3-319-55598-0_7
12. Shetty, S., Kareem, A., & Aithal, G. (2022). Integration of Particle Swarm Optimization and Sliding Mode Control: A Comprehensive Review. In *International Conference on VLSI, Signal Processing, Power Electronics, IoT, Communication and Embedded Systems* (pp. 205–213). Springer, Singapore. https://doi.org/10.1007/978-981-99-4444-6_15
13. Kennedy, J., & Eberhart, R. C. (1995). Particle swarm optimization. In *Proceedings of the IEEE International Conference on Neural Networks* (pp. 1942–1948). IEEE. https://doi.org/10.1109/ICNN.1995.488968
14. Kennedy, J., Eberhart, R. C., & Shi, Y. Y. (2001). *Swarm Intelligence, The Morgan Kaufmann Series in Artificial Intelligence*. Morgan Kaufmann.
15. Shi, Y., & Eberhart, R. C. (1998). A modified particle swarm optimizer. In *Proceedings of the Conference on Evolutionary Computation* (pp. 69–73). IEEE. https://doi.org/10.1109/ICEC.1998.699146
16. Zhu, J., Zhao, J., & Li, X. (2008). A new adaptive particle swarm optimization algorithm. In *2008 International Workshop on Modelling, Simulation and Optimization* (pp. 456–458). IEEE. https://doi.org/10.1109/WMSO.2008.115
17. Deng, X. (11–14 December 2009). *System identification based on particle swarm optimization algorithm*. The 2009 International Conference on Computational Intelligence and Security, Beijing, China. https://doi.org/10.1109/CIS.2009.167
18. Kiencke, U., & Nielsen, L. (2000). Automotive control systems: For engine, driveline, and vehicle. *Measurement Science and Technology*, *11*(12), 1828. https://doi.org/10.1088/0957-0233/11/12/708
19. Damon, P.-M. (2018). *Estimation pour le développement de systèmes d'aide à la conduite des véhicules à deux-roues motorisées* (in French) [PhD Thesis]. Université d'Evry-Val-d'Essonne.
20. Levant, A. (2003). High-order sliding modes: differentiation and output-feedback control. *International Journal of Control*, *76*(9–10), 924–941. https://doi.org/10.1080/0020717031000099029
21. Hedrick, J. K., Rajamani, R., & Yi, K. (1994). Observer Design for Electronic Suspension Applications. *Vehicle System Dynamics, 23*(6), 413–440. https://doi.org/10.1080/00423119408969068
22. Soderstrom, T., & Stoica, P. (1989). *System Identification.* Prentice Hall International.
23. Floret-Pontet, F., & Lamnabhi-Lagarrigue, F. (2001). Parameter Identification Methodology Using Sliding Mode Observers. *International Journal of Control*, *74*(18), 1743–1753. https://doi.org/10.1080/00207170110089761
24. Poli, R., Kennedy, J., & Blackwell, T. (2007). Particle swarm optimization. *Swarm Intelligence*, *1*, 33–57. https://doi.org/10.1007/s11721-007-0002-0
25. Ratnaweera, A., Halgamuge, S. K., & Watson, H. C. (2004). Self-organizing hierarchical particle swarm optimizer with time-varying acceleration coefficient. *IEEE Transactions on Evolutionary Computation*, *8*, 240–255. https://doi.org/10.1109/TEVC.2004.826071

26. World Health Organization. (2018). *Global Status Report on Road Safety 201*8.
27. Observatoire national interministériel de la sécurité routière. (2017). *La Sécurité Routière en France Bilan de l'accidentalité de l'année* (in French).